Shock Waves (2011) 21:141–148
DOI 10.1007/s00193-011-0303-5

ORIGINAL ARTICLE

Hot spot formation from shock reflections

R. Menikoff

Received: 19 July 2010 / Revised: 28 November 2010 / Accepted: 26 January 2011 / Published online: 17 February 2011
© Springer-Verlag 2011

Abstract Heterogeneities sensitize an explosive to shock initiation. This is due to hot-spot formation and the sensitivity of chemical reaction rates to temperature. Here, we describe a numerical experiment aimed at elucidating a mechanism for hot-spot formation that occurs when a shock wave passes over a high-density impurity. The simulation performed is motivated by a physical experiment in which glass beads are added to liquid nitromethane. The impedance mismatch between the beads and the nitromethane results in shock reflections. These, in turn, give rise to transverse waves along the lead shock front. Hot spots arise on local portions of the lead front with a higher shock strength, rather than on the reflected shocks behind the beads. Moreover, the interactions generated by reflected waves from neighboring beads can significantly increase the peak hot-spot temperature when the beads are suitably spaced.

Keywords Hot spots · Shock reflection · Nitromethane

1 Introduction

Most condensed-phase explosives, such as plastic-bonded explosives, are heterogeneous materials. For these explosives, shock initiation is dominated by *hot spots; i.e.*, small localized regions of high temperature that are generated by flow mechanisms such as void collapse, see for example [12]. The ignition and growth concept provides a general description for the reactive processes on the meso-scale of the heterogeneities; see [14] and references therein. However, the details of hot-spot formation and their subsequent evolution are not well understood.

Many mechanisms have been proposed for generating hot spots, see for example [6] and references therein. One hot-spot mechanism that has not received much attention is shock reflection from high-density impurities. This can play an important role in sensitizing liquid or emulsion explosives, as illustrated by the recent experiments of Dattelbaum et al. [2] using doped nitromethane.

Nitromethane is a well-studied homogeneous liquid explosive; see for example [1,3–5]. Adding impurities in a controlled manner results in a well-characterized heterogeneous explosive. Dattelbaum et al. [2] used micron-sized glass beads and microballoons for shock initiation experiments. Their experiments have quantified the change in initiation sensitivity with the size and density of the impurities. However, currently available diagnostic techniques have neither the spatial nor the temporal resolution to measure the evolution of an individual hot spot.

Here, we report on a numerical experiment aimed at elucidating how hot spots are formed when a shock wave interacts with impurities of a higher impedance. Motivated by the experiments of Dattelbaum et al. [2], a non-reactive simulation in two dimensions of a shock wave in nitromethane passing over glass beads is used as an illustrative example. Since glass has a higher acoustic impedance than nitromethane, one expects shock reflections to arise. However, the temperature rise from the shock reflection is relatively small. This is shown in Sect. 2 using an equation of state (EOS) for nitromethane to calculate the Hugoniot loci. Based on general properties of Hugoniot loci of condensed-phase explosives, in the region of interest for shock initiation, reflected shocks are also shown to have a small temperature rise. Thus, when shock heating is the only dissipative mechanism, hot spots

Communicated by B. W. Skews.

R. Menikoff (✉)
Los Alamos National Laboratory, Mail Stop B214,
Los Alamos, NM 87545, USA
e-mail: rtm@lanl.gov

with a substantially higher temperature can only be generated behind local portions of the lead shock front with a higher shock strength.

A detailed study of the numerical results in Sect. 3 reveals that stronger shocks along the lead wave arise for two reasons. First, as the shock sweeps over the glass bead, the angle between the shock front and the interface with the bead increases. At some point there is a transition from regular reflection to Mach reflection. The Mach stem can be thought of as a strong shock on a portion of the lead front. The shocked material behind the Mach stem forms a hot spot. Second, the shock interaction with the beads also generates high pressures which trigger a transverse waves along the lead shock front. A transverse wave is a Mach configuration with the triple point moving along the lead front. Furthermore, if the path of the triple point intersects another bead then the shock reflection off that bead is enhanced. Thus, interactions between neighboring beads can lead to more intense hot spots, either larger size or higher peak temperature.

Transverse waves also play an important role in gaseous detonations, see for example [16]. However, in the gaseous case, an instability in the reaction zone generates the transverse waves and leads to a detonation wave with a cellular structure. For a condensed-phase explosive, the heterogeneities trigger the transverse waves. Since the heterogeneities are random, a cellular detonation would not be expected.

We conclude with a discussion of numerical resolution and accuracy in Sect. 4, followed by a summary of the results of our numerical investigation in Sect. 5. The qualitative features of the flow—Mach reflections and transverse waves along the lead shock front—are quite general. Hence, high impedance impurities in an explosive would provide a source of hot spots for shock initiation and sensitize an explosive.

2 Shock temperature

The shock temperature is determined solely by the material EOS. Our calculations use a Mie–Grüneisen EOS based on the principal shock Hugoniot with a linear u_s–u_p relation as the reference curve, and a constant specific heat for the thermal part; see for example [13]. For nitromethane, we use parameters taken from [11, p. 599] and [10, Table 1.1, p. 5], and listed in the Table 1 below. This simple EOS is readily available and adequate to illustrate the point.

Table 1 Nitromethane EOS parameters

ρ_0	1.125	g/cm^3	Initial density
c_0	1.65	km/s	Initial sound speed
s	1.64	–	$u_s = c_0 + s\,u_p$
Γ_0	0.68	–	Grüneisen coefficient, Γ/V = constant
C_v	1.21	J (g K)$^{-1}$	Specific heat at constant volume

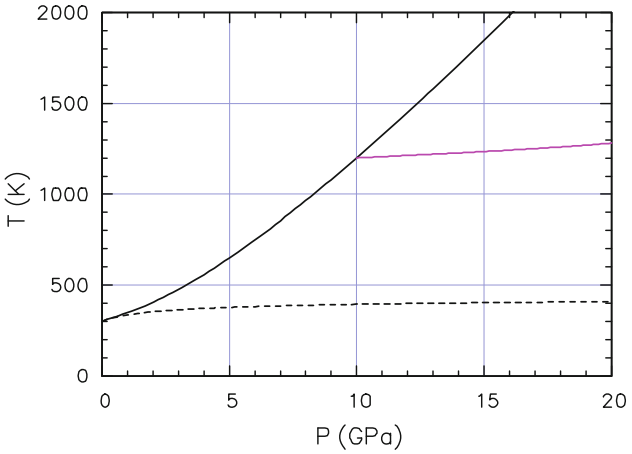

Fig. 1 Temperature along Hugoniot loci in (P, T)-plane for nitromethane; principal Hugoniot is *black curve* and second shock from 10 GPa is *magenta curve*. *Dashed curve* is initial isentrope

The shock and reflected shock temperature as a function of pressure are shown in Fig. 1. We note that the second shock gives rise to only a small increase in temperature. This is typical of condensed-phase explosive in the pressure regime of interest for shock initiation. As shown below, it is a consequence of the high initial sound speed.

The shock temperature can be decomposed into two parts:

$$T(V, S) = T_{S_0}(V) + \Delta T_{\rm irr}(S, V), \tag{1}$$

where V is the specific volume, S is the specific entropy on the Hugoniot locus, and the subscript '0' denotes the value ahead of the shock. The first term is due to isentropic compression to the shock density,

$$T_{S_0}(V) = T_0 \exp\left[-\int_{V_0}^{V} \Gamma \frac{\mathrm{d}V}{V}\right]_{S_0}, \tag{2}$$

where Γ is the Grüneisen coefficient. The second term is from irreversible shock heating,

$$\Delta T_{\rm irr}(S, V) = \int_{S_0}^{S} \left.\frac{T\,\mathrm{d}S}{C_V}\right|_V, \tag{3}$$

where C_V is the specific heat at constant volume. For strong shocks, $P_s \gg P_0$, the shock heating term is much larger than the isentropic compression term, as seen in Fig. 1.

The amount of shock heating for a single strong shock, as compared with that of a double shock to the same final pressure, can be understood by examining the Hugoniot loci in the (V, P)-plane. From the Hugoniot equation,

$$\Delta e = \tfrac{1}{2}(P + P_0)(V_0 - V), \tag{4}$$

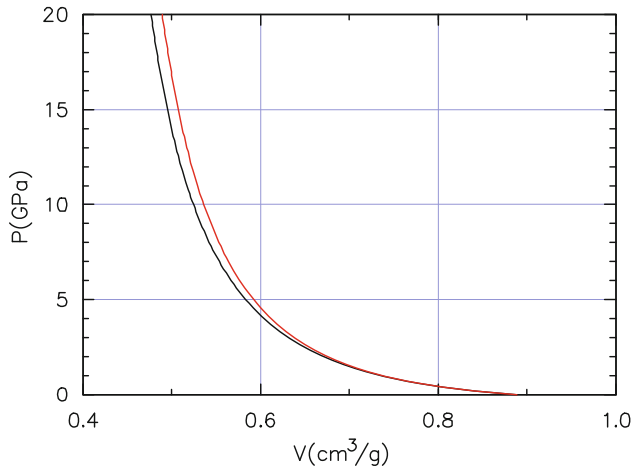

Fig. 2 Loci in (V, P)-plane for nitromethane; *black curve* is isentrope and *red curve* is Huoniot

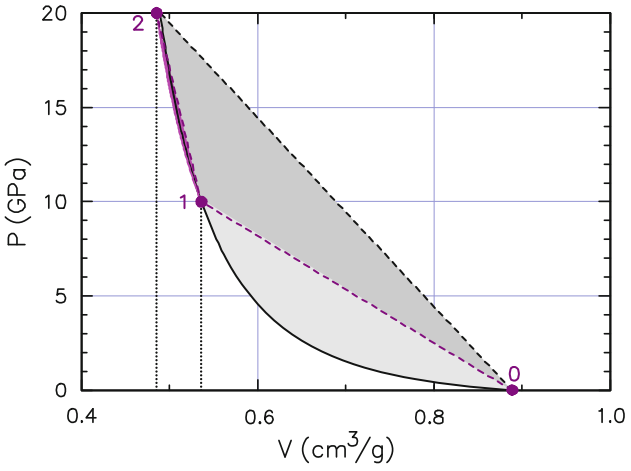

Fig. 3 Nitromethane Hugoniot loci in (V,P)-plane for single strong shock from state 0 to state 2, and sequence of two shocks from state 0 to state 1 to state 2. *Shaded area* in *light gray* and *magenta* correspond to shock heating for the sequence of two shocks. Additional shock heating for single strong shock is shown as *dark gray* area

the change in the specific energy across a shock, Δe, is the area of the trapezoid under the Rayleigh line segment from (V_0, P_0) to (V, P). Due to the high initial sound speed, up to the von Neumann spike pressure, the change in entropy behind the shock is small, even though the pressure ratio P/P_0 is large. Hence, the unreacted Hugoniot locus in the (V, P)-plane is close to the initial isentrope as seen in Fig. 2.

In effect, a small change in compression on the isentrope compensates for the thermal pressure due to shock heating. Consequently, the heating from isentropic compression is approximately the area under the Hugoniot locus. The shock heating can then be approximated by the area between the Rayleigh line and the Hugoniot locus.

For a sequence of two shocks, the entropy change is less than that of a single shock to the same final pressure [7]. Hence, the second Hugoniot locus in the (V, P)-plane is also close to the initial isentrope. The shock heating for the two shocks, shown in Fig. 3, is the area of the light gray and magenta regions. The additional shock heating for the single strong shock is the dark gray area of the triangle formed by the states 0, 1 and 2. Due to the convexity of the Hugoniot locus, this is a large fraction of the heating for the strong shock from state 0 to state 2. Thus, the shock heating for a single shock is much greater than that of two sequential shocks to the same pressure.

This graphical analysis is quite general. Therefore, the small additional temperature rise for a second shock is a general property of condensed-phase explosives. As a result, if shock heating is the only dissipative mechanism, then reflected shocks are not the source of hot spots. We will see in the next section that shock interactions can generate transverse waves along the lead shock front and that high temperatures occur behind portions of the lead front that have a higher shock strength.

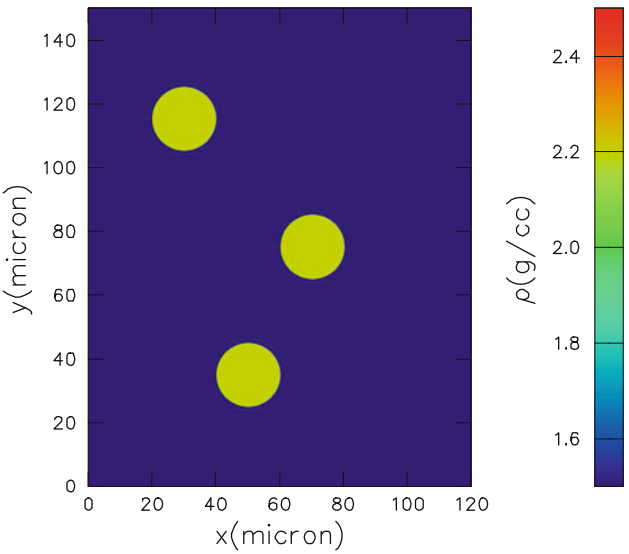

Fig. 4 Initial configuration of simulation. *Blue* corresponds to nitromethane and the three beads are shown in *yellow*. A shock is driven, supported by an inflow boundary condition, and propagates from *left* to *right*

3 Simulation

A two-dimensional hydrodynamic simulation was performed with the xRage code, an Eulerian ASC code at LANL that runs on parallel processors. The initial configuration is shown in Fig. 4. The computational mesh is $120 \times 150\,\mu$m with a cell size of $1/8\,\mu$m. The mesh is initialized with nitromethane (NM) and then three glass beads, $10\,\mu$m in radius centered at (30, 115), (50, 35) and (70, 75), are superimposed. For the glass we use a tabular SESAME EOS for SiO_2 [8, table #7381]. The glass has a higher density than the nitromethane;

2.20 compared with 1.12 g/cm^3. It also has a higher sound speed and hence a higher acoustic impedance.

An inflow boundary condition on the left is used to drive a 10-GPa shock in the nitromethane, propagating from left to right. Reflective boundary conditions are on the top and bottom (effectively, rigid walls). The bead size and shock pressure are comparable to those used in the experiments of Dattelbaum et al. [2]. However, the beads in the experiment are spheres rather than cylinders.

On the meso-scale of material heterogeneities, physical experiments are inherently 3-dimensional, whereas our simulation is only 2-dimensional. Nevertheless, the simulation captures the key features of the shock interactions that lead to the formation of hot spots.

Three points are worth noting. First, the simulation is non-reacting, i.e., the nitromethane is treated as an inert. Based on empirical fits to the reaction rate of nitromethane, see [15], and the peak hot-spot temperature of about 1800 K, the amount of reaction on the 25 ns time scale of the simulation would be small. Second, thermal diffusion is neglected. Typically, for a condensed-phase explosive, the coefficient of thermal diffusion is a few tenths in units of $\mu m^2/\mu s$. Over 25 ns, the diffusion length is less than a cell size. Third, shock heating is the only dissipative mechanism in the simulation.

Consequently, the flow pattern would simply scale with the bead size. Thus, the focus of our simulation is only on the initial shock interactions. The size of the beads becomes important when additional length or time scales are significant. In particular, on a longer time scale then our simulation, reaction becomes important. Experiments show that behind a 10-GPa shock, a detonation wave forms and overtakes the lead shock in about 0.5 μs; see for example [2, Fig. 2]. The adiabatic induction time of the hot spot would be much smaller.

3.1 Shock passing over single bead

The flow as the lead shock sweeps over the first bead is shown in Fig. 5. A key geometric property is that the angle between the shock front and the NM/glass interface varies. As a consequence, the shock interaction starts out as a regular reflection (plot at $t = 5$ ns) and then transits to a Mach reflection ($t = 6.5$ ns). The Mach stem can be thought of as a portion of the lead front with a higher shock strength and hence gives rise to a region of high temperature on each side of the bead.

Subsequently, as the shock angle continues to increase on the downstream side of the bead, the shock front adjacent to the bead weakens ($t = 8.0$ ns). Due to the expanding reflected shock from the upstream side of the bead, the pair of Mach triple points moves away from the bead along the lead front; i.e., the interaction of the shock with the bead triggers a transverse wave along the shock front.

Finally, when the transmitted shock breaks out of the bead, a region of low pressure is formed on the downstream side of the bead ($t = 9.0$ ns). Consequently, there is only a localized hot spot in the regions where the Mach stem first formed. In addition, there is a band of relatively high temperature that follows the path of a triple point. However, the temperature of the band decreases as the reflected wave expands and weakens.

As discussed in the previous section, there is only a small temperature rise behind the bead due to the reflected shock. High temperatures only arise along local portion of the lead front that have a higher shock strength.

3.2 Interactions from multiple beads

The reflected waves from multiple beads can interact and enhance the generation of hot spots. This is illustrated by the flow of the lead shock over the third bead shown in Fig. 6. The bands in the temperature plot at $t = 13$ ns indicate the path of the triple points for the transverse waves set up by the shock reflections from the first two beads. These paths intersect the third bead. Consequently, the higher lead shock strength from the transverse wave strengthens the reflection off the third bead, as seen in the pressure plot at $t = 15$ ns.

The asymmetry in the relative spacing of the beads gives rise to an enhanced hot spot (larger size and higher peak temperature) on the bottom relative to the top of the third bead, as seen in the temperature plot at $t = 17$ ns. This is because the triple point from the bottom bead intersects the third bead closer to where the transition to Mach reflection occurs than does the triple point from the top bead.

We note that the shock interaction with one bead can also weaken the reflection at the next bead. For instance, this would occur if the downstream bead is in the shadow of a previous bead, i.e., at a position for which the lead shock pressure is decreased. Thus, depending on their relative positions, the interactions between beads can be either constructive or destructive.

Due to the divergence of a reflected wave, the beads need to be within a few diameters for their interactions to have an appreciable affect on hot spot formation. Furthermore, the divergence effect would be stronger for physical materials, in which the impurities are inherently 3-dimensional, than are displayed in the 2-dimensional simulation shown here.

3.3 Flow behind lead front

At the end of the simulation, just before the shock reaches the right boundary at $t = 24.5$ ns, the beads are well behind the lead front as shown in Fig. 7. Several points are worth noting. Despite the multiple shock interactions from the reflections off the beads and the top and bottom boundaries, the temperature behind the beads is nearly the same as the incident shock

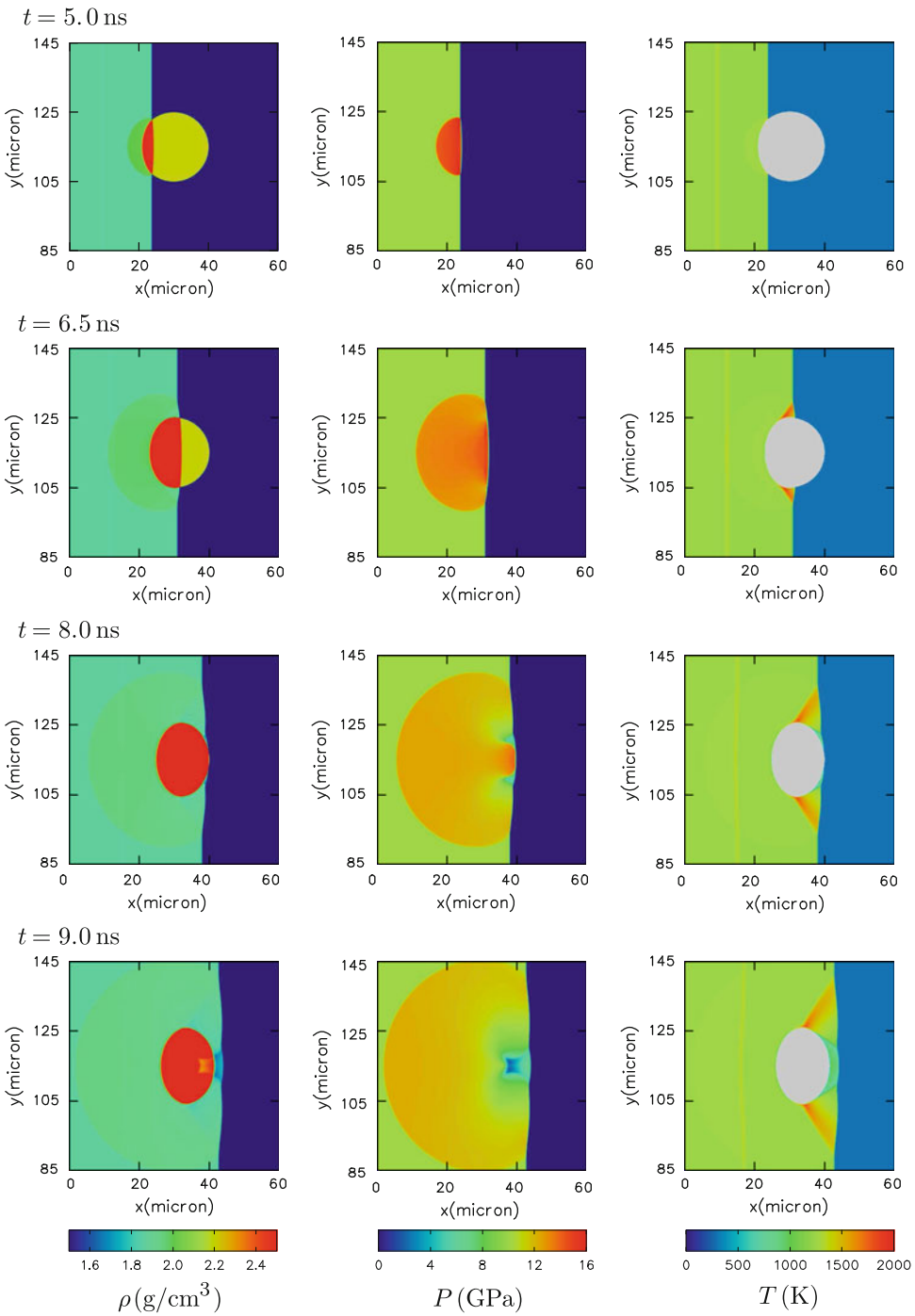

Fig. 5 Time sequence of density, pressure and temperature as the lead shock sweeps over first bead. Region of glass bead is grayed out on temperature plots

temperature. This emphasizes the point that hot-spot formation requires dissipation and does not result from isentropic compression. Moreover, multiple shocks have much less dissipation than a single shock to the same final pressure.

The downstream side of beads are severely distorted, and lead to localized regions with very high vorticity. Moreover, the high vorticity occurs in the same regions as do the hot spots. When the hot spots react, they generate high temperatures and trigger deflagration wavelets. Very likely the vorticity would lead to entrainment of reactant with the hot products, i.e., turbulent mixing. This could enhance the deflagration speed over that which would occur from heat conduction alone; see for example [9]. Another implication of the vorticity is that late time calculations of the flow would require an Eulerian mesh since a Lagrangian mesh would suffer from grid tangling.

Finally, we note that the distortion of the lead front has a displacement amplitude which is very small compared

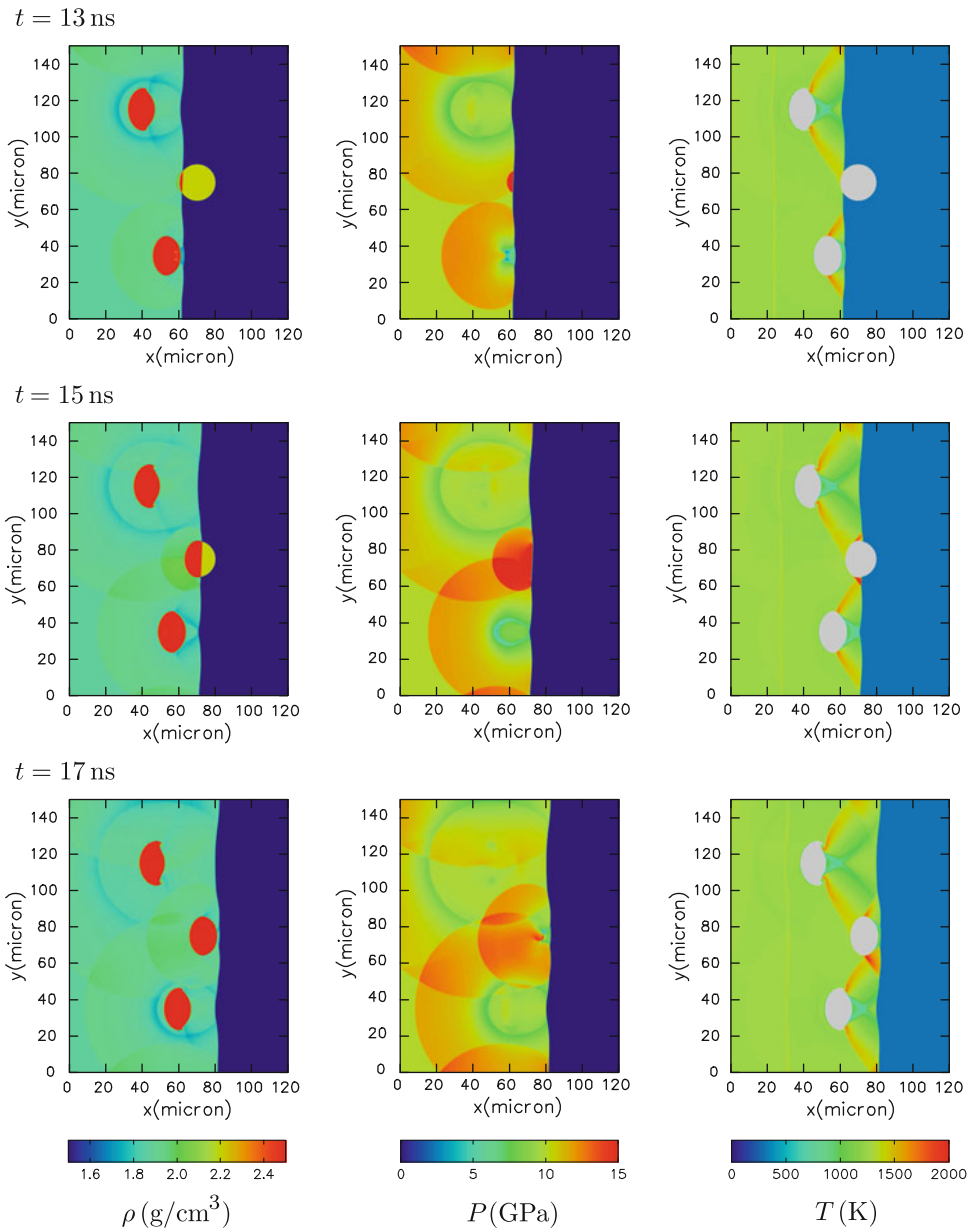

Fig. 6 Time sequence showing enhanced shock interaction with the *middle bead* due to reflected waves from the adjacent two beads. Glass beads are grayed out on temperature plots

with the size of the beads. In contrast to the fingering that occurs at material interfaces for unstable flows, such as due to Richtmyer–Meshkov instability, the high sound speed resulting from the high shock pressure causes perturbation to trigger transverse waves along the lead front.

However, despite the near-planarity of the front, there are large pressure variations along it. This can have important consequences when the lead wave hits an interface. One illustrative example occurs for VISAR measurements of the velocity time history behind a shock or detonation wave in a plastic-bonded explosive (PBX). Typically, a reflective aluminum layer is placed between the PBX and a window. If the aluminum layer is too thin or not protected with a plastic layer, then the reflected laser light signal is lost when the wave impacts the interface. This is indicative of the pressure variation at the wave front breaking up the reflective layer. Thus, one should not assume that planarity within measurement accuracy (currently limited to simultaneity within about 1 ns) implies uniformity of the lead shock front.

4 Discussion of numerics

The simulation reported in the previous section used a fairly high resolution with a uniform mesh of 960×1200 cells, and required about 2000 cycles, based on the lead shock speed and a CFL number of 0.5. The shock interaction with a single bead shown in Fig. 5 corresponds to a 480×480 submesh.

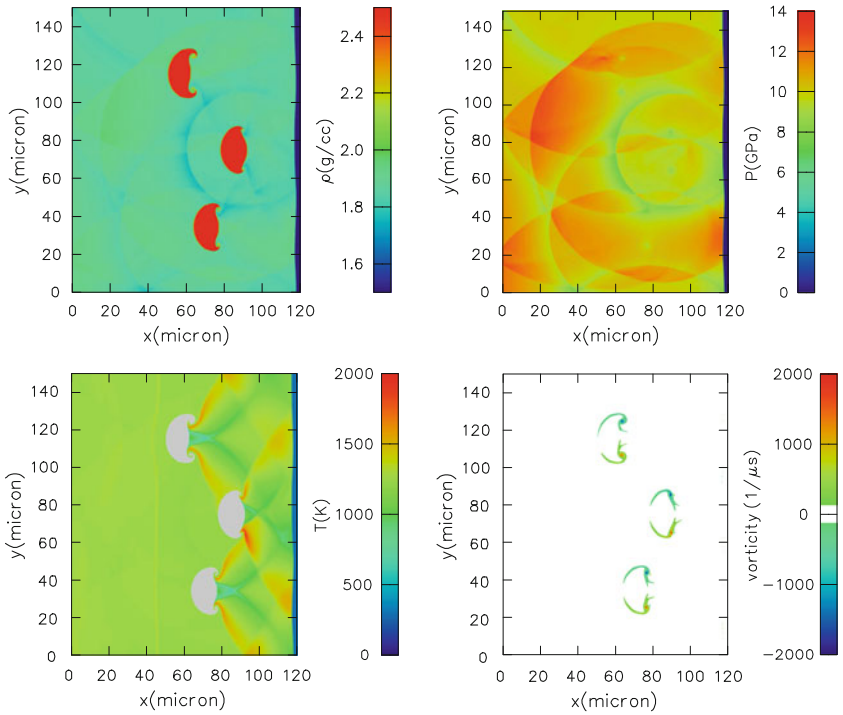

Fig. 7 Flow at end of the simulation, after the lead shock has past the beads and just before shock reaches right boundary, $t = 24.5$ ns. Glass beads are grayed out on temperature plot

Across the bead diameter, which is the natural geometric length scale, there were 160 cells. This grid allows the Mach stem and the hot spot, which are a small fraction of the bead diameter, to be adequately resolved as seen in the subplots at $t = 6.5$ ns of Fig. 5.

With half the resolution, the pressure field would be nearly the same. This is because acoustic waves rapidly equilibrate the pressure and velocity. The temperature field is less accurate due to numerical diffusion associated with advection. This can have a large effect on hot spots as the peak temperature can be significantly degraded on a coarse mesh.

The xRage code has an adaptive mesh capability. This was not used since the adaptation criterion aims at resolving pressure gradients. Coarsening the mesh behind a shock wave is a smoothing operation and results in numerical diffusion for the temperature field which would smear out the hot spots.

The nature of the flow is such that there are cumulative errors at late time that degrade the accuracy of some aspects of the numerical solution. In particular, as seen in Fig. 7, the large local gradients in the velocity field due to the vorticity on the downstream side of the beads are not well resolved and are very likely subject to a Kelvin–Helmholtz type of physical instability that would at later times lead to a von Kármán vortex street. The vorticity also gives rise to a large distortion on the downstream side of the beads, and the distorted portion of the interface may be inaccurate.

The intent of the simulation is to illustrate the flow as a shock wave passes over high impedance impurities. The simulation is sufficiently accurate to show the mechanism by which hot spots are formed. Moreover, though the details of the flow would depend on the EOS of the specific materials used, the general features of the shock interactions leading to hot spots would be the same for a wide class of condensed-phase explosives.

5 Summary

The key results on hot-spot formation from the shock interaction with a high impedance impurity can be summarized as follows:

(i) The temperature rise from a reflected shock is very small compared with that of the lead shock.
(ii) Significantly higher temperatures arise from a stronger shock along a portion of the lead front. This results from a transverse wave or a Mach configuration. The region of shocked material behind the Mach stem forms the hot spot.
(iii) Higher temperature hot spots can result from constructive interference of shock interactions with neighboring beads. This occurs when the path of a triple point generated by one bead intersects a downstream bead. In addition, beads need to be close enough such that the divergence effect of a reflected wave is not too large. This requires a sufficiently high number density of beads.
(iv) The flow over a bead generates significant vorticity. Entrainment of hot products with the reactants is likely

to enhance the burn rate. This would be similar to turbulent mixing that occurs for gaseous detonation; see [16].

(v) The displacement amplitude of the lead front is small; i.e., only a fraction of the radius of the beads. However, the pressure variation along the front may be large.

The high temperature of the hot spots would lead to rapid reaction and thermal runaway on a fast time scale of $\sim$100 ns. This is expected to trigger deflagration wavelets emanating from the hot spots. The chemical energy released is then acoustically coupled to the lead front. This provides the feedback that causes the shock to strengthen and then transit to a detonation wave as is observed in experiments; see for example [2, Fig. 6].

The nature of the heterogeneities along with the hot-spot generating mechanism affects the hot-spot distribution (temperature and volume), and hence the sensitivity of an explosive to shock ignition. For example, experiments have observed that nitromethane doped with hollow glass beads (microballoons) is more sensitive than when doped with solid glass beads, for the same size distribution and number density of beads [2].

Simulating the evolution of hot spots, subsequent reaction and the coupling of the energy released to the shock front would be the logical next step for understanding shock initiation. However, this is computationally very challenging because of the multiple spatial and temporal scales associated with the hydro flow and the chemical reaction.

Acknowledgments This work was carried out under the auspices of the U. S. Department of Energy at LANL under contract DE-AC52-06NA25396 as part of LDRD project on hot spots (project #20080015DR).

References

1. Blais, N.C., Engelke, R., Sheffield, S.A.: Mass spectoscopic study of the chemical reaction zone in detonating liquid nitromethane. J. Phys. Chem. A **101**, 8285–8295 (1997)
2. Dattelbaum, D.M., Sheffield, S.A., Stahl, D.B., Dattelbaum, A.M., Trott, W., Engelke, R.: Influence of hot spot features on the initiation characteristics of heterogeneous nitromethane. In: Fourteenth Symposium (International) on Detonation (2010)
3. Engelke, R.: Effect of a chemical inhomogeneity on steady-state detonation velocity. Phys. Fluids **23**, 875–880 (1980)
4. Engelke, R., Earl, W.L., Rohlfing, M.: Microscopic evidence that the nitromethane aci ion is rate controlling species in the detonation of liquid nitromethane. J. Chem. Phys. **84**, 142–146 (1986)
5. Engelke, R., Sheffield, S.A., Stacy, H.L.: Effect of deuteration on the diameter-effect curve of liquid nitromethane. J. Phys. Chem. A **110**, 7744–7748 (2006)
6. Field, J.E., Bourne, N.K., Palmer, S.J.P., Walley, S.M.: Hot-spot ignition mechanisms for explosives and propellants. Phil. Trans. R. Soc. Lond. A **339**, 269–283 (1992)
7. Henderson, L.F., Menikoff, R.: Triple-shock entropy theorem and its consequences. J. Fluid Mech. **366**, 179–210 (1998)
8. Holian, K.S.: T-4 Handbook of material property data bases. Vol. Ic equations of state. Technical Report LA-10160-MS, Los Alamos National Lab (1984)
9. Karpenko, I.I., Morozov, V.G., Chernysheva, O.N., Yanilkin, Y.V.: Calculations of rate of growth of hot spots during detonation taking into account the turbulent mechanism of energy transfer. Russ. J. Phys. Chem. B **2**, 157–161 (2008)
10. Mader, C.L.: Numerical Modeling of Explosives and Propellants, 3rd edn. CRC Press, Boca Raton (2008)
11. Marsh, S.P. (ed.): LASL Shock Hugoniot Data. University of California Press, Berkeley (1980)
12. Menikoff, R.: Pore collapse and hot spots in HMX. In: Shock Compression of Condensed Matter 2003, pp. 393–396 (2004)
13. Menikoff, R.: Empirical equations of state for solids. In: Y. Horie (ed.) Solids I. Shock Wave Science and Technology Reference Library, vol. 2, Chap. 4. Springer-Verlag, Berlin (2007)
14. Menikoff, R.: On beyond the standard model for high explosives: challenges & obstacles to surmount. In: Shock Compression of Condensed Matter 2009, pp. 18–25 (2009)
15. Menikoff, R., Shaw, M.S.: Modeling detonation waves in nitromethane. (2010, in preparation)
16. Radulescu, M.I., Sharpe, G.J., Law, C.K., Lee, J.H.S.: The hydrodynamic structure of unstable cellular detonations. J. Fluid Mech. **580**, 31–81 (2007)